Available online at www.sciencedirect.com
ScienceDirect
Catalysis Today 118 (2006) 353–359
CATALYSIS TODAY
www.elsevier.com/locate/cattod

Alumina-supported V–Mo–O mixed oxide catalysts, the formation of phases involving aluminum: $AlVMoO_7$

S.J. Khatib, R. Guil-López, M.A. Peña, J.L.G. Fierro, M.A. Bañares *

Instituto de Catálisis y Petroleoquímica, CSIC, Marie Curie 2, Cantoblanco, 28049 Madrid, Spain

Available online 22 August 2006

Abstract

The structure and reactive properties of alumina-supported molybdena, vanadia and molybdena–vanadia above monolayer coverage are studied by XPS, XRD, Raman spectroscopy and methanol temperature-programmed surface reaction (TPSR). Alumina-supported series are prepared by impregnation. Reference bulk Mo–V–Al oxide systems are prepared. The bulk Mo–V–Al oxide system provides structural references to characterize the alumina-supported series. The Raman bands of $AlVMoO_7$ are reported here for the first time, to the best of our knowledge. It is shown that the chemistry of the bulk Al–V–Mo system is also present in the alumina-supported Mo–V oxide catalysts. Methanol TPSR data show that the systems possess essentially redox activity.

Keywords: $AlVMoO_7$; Mixed Al–V–Mo oxides; Oxidation; Methanol; Raman; XRD; XPS

1. Introduction

The oxidative dehydrogenation (ODH) of light alkanes has proved to be an attractive route to obtain their valuable olefin counterparts. The catalysts used for this reaction of selective oxidation are usually V and Mo oxides, though typically vanadium is the key element associated to higher rates and olefin selectivities [1–8]. Studies with bulk mixed metal oxides show that these are efficient catalysts for alkane oxidation to olefins, oxygenates and nitriles [1,3–8]. The nature of the active phase on the surface of these bulk mixed metal oxides is difficult to study and as yet, remains unknown. It is therefore important to study the surface of these mixed oxides and reach a better understanding of the nature of the active sites. Alumina-supported molybdenum and alumina-supported vanadia catalysts typically present surface oxide species below monolayer and segregated crystalline MoO_3 or V_2O_5 phases above monolayer.

The chemistry of the two elements below monolayer has been studied in detail [9,10]. Mo has no structural effect on V catalysts, but it can have an effect on reactivity in some reactions where the presence of the second element has a clear promoting effect [11,12]. This is explained by a promotion of the acidic properties of the system, which promotes the adsorption of reactants, like in the selective catalytic reduction of NO_x by ammonia [11]. Propane ODH shows some moderate promoting effect by the coexistence of dispersed vanadia and molybdena below monolayer coverage [10]. Typically the promoting effect in Mo, V-containing catalysts appears associated to the presence of mixed Mo–V–O phases [3,6,8,10,13]. The presence of both Mo and V in the same system does promote reactivity. However, the exact nature of the active phase in bulk Mo–V–O phases is not clear since most efforts concentrate on the bulk structure of these oxides; however, molecules interact with the outermost layer, directly exposed to the reactant. The outermost layer is the termination of the bulk regular structure, and will not be like the bulk. In addition, the actual structure of the outermost layer must be reconstructed during reaction, rendering the actual active phase, in line with other systems [14]. It is possible that the nature of the species present at the surface of Mo–V oxide catalysts in the submonolayer region and in the bulk phase be similar, in line with other studies that underline the close relationships between bulk and supported oxides [15–17].

Mixed Mo–V oxide catalysts show particularly efficient performance for propane oxidation to propylene [5–8]. Previous studies carried out in our laboratories showed that when preparing alumina supported Mo + V oxide catalysts with a loading above monolayer coverage, a mixed Mo–V phase

* Corresponding author. Tel.: +34 91 585 4788; fax: +34 91 585 4760.
E-mail address: banares@icp.csic.es (M.A. Bañares).

0920-5861/$ – see front matter © 2006 Elsevier B.V. All rights reserved.
doi:10.1016/j.cattod.2006.07.023

characterized by Raman bands at 770 and 230 cm^{-1} appears [10]; such phase has also been observed by Bell et al. [13]. It should be a mixed Mo–V oxide phase, and it may involve some Al cations from the support; however, no clear assignment of these bands has been made for the so called ''phase I'' yet. The aim of this work is to prepare high loading Mo–V oxide catalysts on alumina and reference Al–V–Mo oxide to identify ''phase I'', which displays a good catalytic behavior [10]. Methanol probe reaction is used to determine the reactivity of their surface sites.

2. Experimental

2.1. Preparation of references and catalysts

The reference bulk-MoVAl mixed oxide sample (phase I) was prepared using the ceramic method by grinding the simple molybdenum, vanadium and aluminum oxides at atomic ratio Mo:V:Al = 1:1:1 [18]. The ground mixture was heated at 550 °C for 24 h (sample bulk-MoVAl-24) and for 48 h (sample bulk-MoVAl-48).

Alumina-supported Mo, V and Mo–V mixed oxide catalysts were prepared with different loadings of the metal oxides and at a constant Mo/V = 1 atomic ratio. Total loading was 18 and 45 atoms/nm^2 of alumina support. This value is calculated with respect to the area of the alumina support. This loading is above monolayer coverage, ca. 8 atoms/nm^2 for surface vanadia and ca. 5 atoms/nm^2 for surface molybdenum oxide [19]. Thus, the amount is equivalent to ca. 2–3 monolayers on alumina for 18 MoVA and 5–6 monolayers on alumina for 45MoVA, which warrants the formation of nano-scaled crystalline phases. The precursors were NH_4VO_3 (Sigma–Aldrich) and $(NH_4)_6Mo_7O_{24}{\cdot}4H_2O$ (Merck). A γ-Al_2O_3 (Engelhard) with a specific surface area of 222 $m^2\ g^{-1}$ was employed as support. The samples were prepared by impregnation with an aqueous solution of the precursors and treated in a rotary evaporator at 80 °C at 0.8 atm. In the case of the supported mixed oxide catalysts, both Mo and V were coimpregnated by a mixture solution containing both precursors. The impregnated solids were dried at 120 °C for 1 h and then calcined at 450 °C for 5 h, under air flow. The catalysts are labeled as *x*MoVA, *x*MoA and *x*VA, where *x* indicates the total number of Mo + V atoms per square nanometer of the alumina support. Table 1 shows the catalysts prepared and their compositions.

Table 1
Nomenclature and compositions of the molybdena and/or vanadia alumina supported samples: 18MoA, 18VA, 18MoVA and 45MoVA samples

Catalyst	Support	Mo and V loadings	
		(Mo + V)[a]	Mo:V
18VA	Al_2O_3	0 + 18	0:1
18MoA	Al_2O_3	18 + 0	1:0
18MoVA	Al_2O_3	9 + 9	1:1
45MoVA	Al_2O_3	22.5 + 22.5	1:1

[a] Metal surface density: metal atoms/nm^2 of alumina support.

2.2. X-ray diffraction

X-ray diffraction patterns were recorded using a Seifert 3000XRD diffractometer using Cu Kα radiation in scan mode (0.02°, 2 s). The crystalline phases were identified using the Joint Committee of Powder Diffraction Standards (JCPDS) files.

2.3. Raman spectroscopy

Raman spectra were run with a single monochromator Renishaw System 1000 equipped with a thermoelectrically cooled CCD detector (−73 °C) and holographic super-Notch filter. The samples were excited with the 633 nm He–Ne line; spectral resolution was ca. 3 cm^{-1} and the spectrum acquisition time was 300 s. The spectra were obtained under dehydrated conditions (at 120 °C after pretreatment at 350 °C in dry synthetic air during 30 min) in an *in situ* cell (Linkam TS-1500).

2.4. Photoelectron spectroscopy

X-ray photoelectron spectra (XPS) were recorded on a VG ESCALAB 200R spectrometer equipped with a hemispherical electron analyzer, using a Mg Kα ($h\nu$ = 1253.6 eV, 1 eV = 1.603 × 10^{-19} J) X-ray source. Peak intensities were estimated by calculating the integral of each peak, after subtraction of a Shirley background, and fitting the experimental curve to a combination of Lorentzian and Gaussian curves. For each sample, Al 2p, Mo $3d_{5/2}$, V $2p_{3/2}$, O 1s and C 1s core-level spectra were recorded. All binding energies (BE) are referred to the C 1s line at 284.6 eV.

2.5. Methanol temperature programmed surface reaction (TPSR) profiles

The reactive nature of the surface sites at the alumina-supported catalysts was tested by the temperature-programmed surface reaction (TPSR) profiles of chemisorbed methanol. The catalysts (0.125 g) were placed in a quartz tubular reactor with a coaxially centered thermocouple of a temperature-programmed system equipped with an on-line mass spectrometer with a quadrupole detector (Balzers QMG 125). Prior to reaction the catalysts were activated in flowing synthetic air at 450 °C for 1 h, then cooled to 100 °C and switched to a flowing stream of Ar/He (5% Ar in He) during 1 h to flush out the residual gas phase O_2. Methanol chemisorption process was carried out at 100 °C [17,20] by switching a flow of 60 ml min^{-1} of methanol (2000 ppm CH_3OH/5% Ar in He). The chemisorption process was monitored to control the complete methanol saturation of the active centers of each catalyst (different chemisorption time for each catalyst). The system was then purged with flowing Ar/He during another hour at 100 °C. Then, the catalysts were heated at two different constant heating rates to 500 °C in flowing 5% He/Ar, with two different He/Ar flows. So, two different surface thermo-program conditions [1,2] were chosen to carry out this test of oxidation capacity depending on the

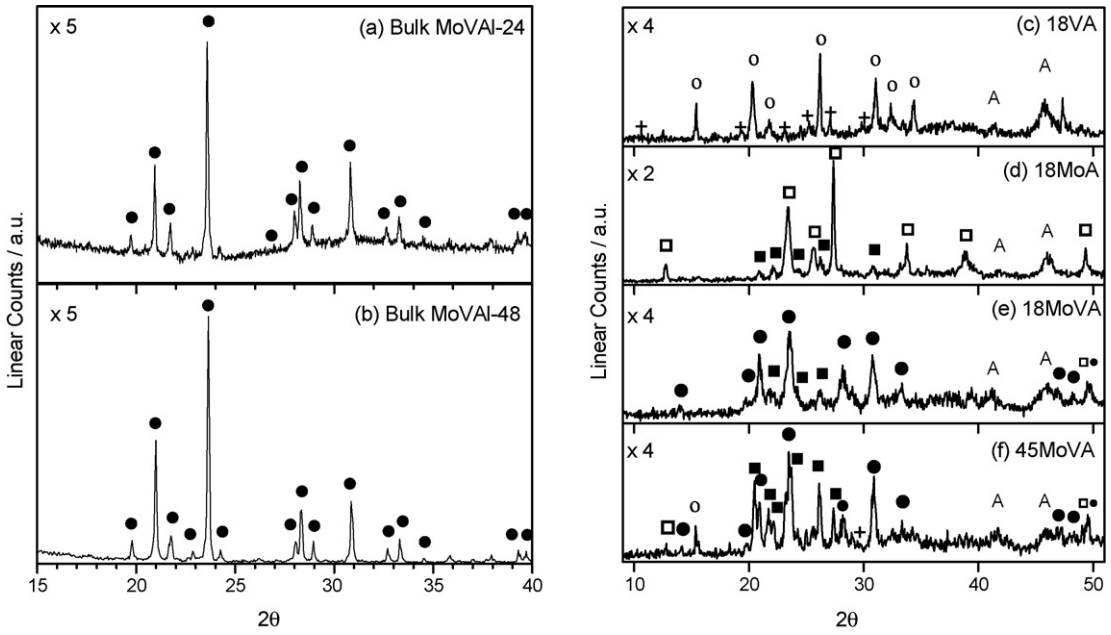

Fig. 1. XRD patterns of bulk-MoVAl samples (left panel): (a) MoVAl-24; (b) MoVAl-48 and of the fresh calcined Mo–V supported catalysts (right panel); (c) 18VA; (d) 18MoA; (e) 18MoVA; (f) 45MoVA. Phase identification: (○), V_2O_5; JCPDS file: 77-2418; (+), AlV_3O_9; JCPDS file: 49-694; (□), α-MoO_3; JCPDS file: 35-609; (■), $Al_2(MoO_4)_3$; JCPDS file: 23-764; (●), $AlVMoO_7$; JCPDS file: 46-687. (A), alumina support. The diffraction patterns have been expanded by the factor indicated in each figure.

sensitivity of the measurement required. Reaction condition #1 was designed for the different metal oxide catalysts, which show big differences in their behaviour: 18VA, 18MoA and 18MoVA (heating rates of 10 °C min^{-1} and 5% He/Ar flow of 60 ml min^{-1}). Reaction condition #2 was designed to study the mixed oxide catalysts with different loadings, for which a high sensitivity in the measurements is required: 18MoVA and 45MoVA (heating rates of 5 °C min^{-1} and 5% He/Ar flow of 150 ml min^{-1}). The primary reaction products are formaldehyde, dimethyl ether (DME) and CO_2, produced on redox, acidic and basic sites, respectively. CO is a secondary product and water is produced in all the processes. Therefore, no data shall be reported on CO and H_2O evolution. Dimethoximethane and methyl formate production is negligible in these samples.

The mass-to-charge (m/z) ratios employed for the identification were methanol (CH_3OH) reagent $m/z = 31$, formaldehyde (HCHO) $m/z = 30$, water $m/z = 18$, CO $m/z = 28$, CO_2 $m/z = 44$ and dimethyl ether (DME) $m/z = 45$. To eliminate errors due to changes in pressure within the ionization chamber of the spectrometer, all signals were ratioed to the Ar [$m/z = 40$] signal.

3. Results

3.1. X-ray diffraction (XRD)

Fig. 1 shows the X-ray diffractograms of the bulk samples and of the supported catalysts. The XRD pattern of bulk MoVAl-24 (Fig. 1a) is characteristic of the ternary mixed phase: $AlVMoO_7$ (JCPDS file 46-687), if bulk MoVAl is heated at 550 °C during 24 h more (MoVAl 48), the lines of $AlVMoO_7$ sharpen and new lines of segregated $Al_2(MoO_4)_3$ appear (Fig. 1b). All the alumina-supported catalysts exhibit the diffraction pattern of γ-Al_2O_3. 18VA exhibits the diffraction pattern of V_2O_5 (JCPDS file 77-2418) and trace amounts of AlV_3O_9 (JCPDS file 49-694) (Fig. 1c). 18MoA presents the diffraction pattern of α-MoO_3 (JCPDS file 35-609) and a weak pattern of $Al_2(MoO_4)_3$ (JCPDS file 23-764) (Fig. 1d). 18MoVA diffraction pattern is dominated by that of $AlVMoO_7$ (JCPDS file 46-687), plus a weak pattern of $Al_2(MoO_4)_3$ (JCPDS file 23-764) (Fig. 1e). The diffraction pattern of $Al_2(MoO_4)_3$ increases with respect to that of $AlVMoO_7$ with coverage in 45MoVA, where some traces of MoO_3 and V_2O_5 become apparent (Fig. 1f). The diffraction lines of the γ-Al_2O_3 weaken with Mo-V loading, which may be due to a dilution effect of the alumina and to the loss of crystallinity due to the migration of Al cations into new phases formed by reaction between the supported oxides and alumina support. Table 2 lists

Table 2
Summary of phases observed by XRD and Raman spectroscopy in the bulk references and alumina-supported catalysts

Sample	Raman	XRD
Bulk MoVAl-24	(760, 230, 203 cm^{-1})[a] $Al_2(MoO_4)_3$	$AlVMoO_7$ (not observed)
Bulk MoVAl-48	(760, 230, 203 cm^{-1})[a] $Al_2(MoO_4)_3$	$AlVMoO_7$ $Al_2(MoO_4)_3$
18VA	V_2O_5	V_2O_5
18MoA	MoO_3	MoO_3
18MoVA	(760, 230 cm^{-1})[a] $Al_2(MoO_4)_3$ V_2O_5 (traces)	$AlVMoO_7$ $Al_2(MoO_4)_3$ (not observed)
45MoVA	(760, 230 cm^{-1})[a] $Al_2(MoO_4)_3$ V_2O_5, MoO_3 weak	$AlVMoO_7$ $Al_2(MoO_4)_3$ V_2O_5, MoO_3weak

[a] Raman bands currently not assigned in literature; this paper associates them to $AlVMoO_7$.

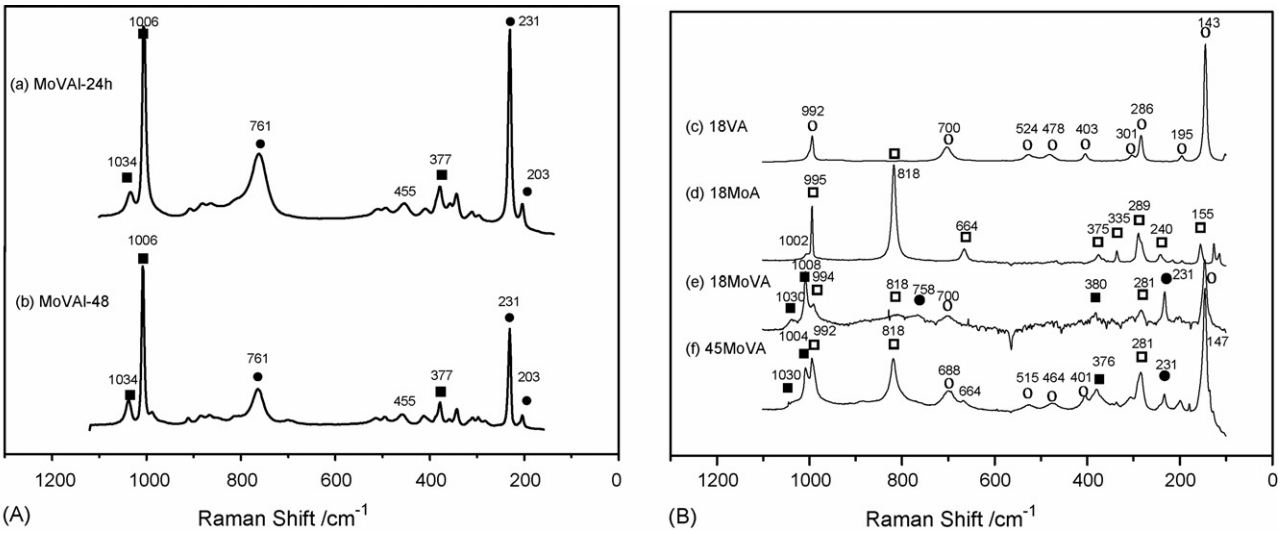

Fig. 2. Raman spectra of bulk-MoVAl samples (left panel): (a) MoVAl-24; (b) MoVAl-48 and of the fresh calcined and dehydrated alumina-supported catalysts (right panel); (c) 18VA; (d) 18MoA; (e) 18MoVA; (f) 45MoVA. Phase identification: (○), V_2O_5; (+), AlV_3O_9; (□), α-MoO_3; (■), $Al_2(MoO_4)_3$; (●), $AlVMoO_7$.

the phases (dominant, secondary and traces) observed by XRD and Raman spectroscopy.

3.2. Raman spectroscopy

3.2.1. Reference of mixed bulk phase

The Raman spectrum of the sample bulk-MoVAl exhibits two collections of Raman bands (Fig. 2a). The bands at 1034, 1006 cm^{-1} and a weak band at 377 cm^{-1} are not sensitive to hydration; their position and relative intensities correspond to $Al_2(MoO_4)_3$ [21–23]. It is difficult to confirm or rule out the presence of surface V or Mo oxide species, characterized by the Raman modes of V=O (1030 cm^{-1}) and Mo=O (1000 cm^{-1}). These could be overshadowed by the very intense Raman bands of $Al_2(MoO_4)_3$ at 1034 and 1006 cm^{-1}. The Raman bands at 761, 231 and 203 cm^{-1} have not been described until present and are not sensitive to hydration. Therefore, they correspond to a crystalline phase. The intensity of the Raman bands at 761, 231 and 203 cm^{-1} decrease with respect to those of $Al_2(MoO_4)_3$ for MoVAl-48 (Fig. 2b).

3.2.2. Alumina-supported catalysts

18VA (Fig. 2c) shows the Raman bands of V_2O_5 crystals (994, 701, 525, 409, 295, 285, and 143 cm^{-1}), while the sample 18MoA (Fig. 2d) exhibits Raman bands that are characteristic of α-MoO_3 crystals (999, 820, 672, 383, 342, 290, 250, and 163 cm^{-1}). Both 18MoA and 18VA have a metal oxide loading above the monolayer coverage and therefore three-dimensional crystallites of α-MoO_3 and V_2O_5 form, which is in line with XRD results.

The supported mixed oxide samples, 18MoVA (Fig. 2e) and 45MoVA (Fig. 2f), exhibit the Raman bands of MoO_3 and V_2O_5, but these are weaker. In addition weak Raman bands at 1034, 1008 and 380 cm^{-1} underline the presence of $Al_2(MoO_4)_3$; the stronger new Raman bands observed in the MoVAl samples at 758 and 231 cm^{-1} are present. These new bands become more intense for 18MoVA than 45MoVA.

3.3. X-ray photoelectron spectroscopy (XPS)

Table 3 illustrates the XPS characterization data. The binding energies of the principal peaks are summarized for Al 2p, Mo $3d_{5/2}$ and V $2p_{1/2}$. The V 2p core level is centered at 517.2 eV, typical of V^{5+} species surrounded by oxygen species [24]. The Mo $3d_{5/2}$ peak is centered at 232.6 eV, characteristic of Mo^{6+} ions in oxygen environment [24]. The coexistence of Mo and V at the surface does not have a clear effect on their BE values; therefore, Mo and V exhibit the highest oxidation state in all the catalysts; which is consistent with the phases detected in the bulk MoVAl oxide phase.

Table 3 also presents the atomic M/Al ratios determined by XPS. The V/Al atomic ratio for 18VA is 0.44. The M/Al ratio is lower for 18MoA (0.21) and 18MoVA (0.29), which possess the same surface loading of supported oxide. So, the atomic M/Al

Table 3
Binding energies (eV) of core electrons of Mo–V samples and surface atomic ratios of 18MoA, 18VA, 18MoVA, and 45MoVA catalysts

Samples	Al 2p	Mo $3d_{5/2}$	V $2p_{3/2}$	Mo/Al at.	V/Al at.	(Mo + V)/Al at.	Mo/V at.
18VA	74.6	–	517.2	–	0.44	0.44	0
18MoA	74.5	232.6	–	0.21	–	0.21	–
18MoVA	74.4	232.6	517.3	0.16	0.12	0.29	1.34
45MoVA	74.4	232.7	517.0	0.10	0.16	0.26	0.63
Bulk-MoVAl-24	74.7	233.1	517.6	1.25	1.40	2.65	0.89

Table 4
Methanol TPSR data on the alumina-supported catalysts

TPSR program[a]	Samples	HCHO			DME		CO_2	
		Area[b] (a.u.)	T_{onset}[c] (°C)	T_{max}[d] (°C)	Area[b] (a.u.)	T_{max}[d] (°C)	Total area[b] (a.u.)	T_{max}[d] (°C)
Reaction condition #1	18VA	1.05	149	215	0.013	215	0.15	260, 305, 400
	18MoA	0.36	153	205	0.004	205	0.05	213, 335, 430
	18MoVA	1.41	125	200	0.031	190	0.14	310, 415
Reaction condition #2	18MoVA	0.46	134	205	0.011	190	0.04	320
	45MoVA	0.27	147	210	0.003	190	0.06	330

[a] Reaction conditions 1 and 2 have been described in Section 2.
[b] Area under the [*m*/*z*] mass signal profiles.
[c] T_{onset}, temperature (in °C) at which the Ar-normalized [*m*/*z*] of HCHO reach the value: 5×10^{-4} a.u.
[d] T_{max}, temperature (in °C) at which the profiles reach their maximum.

ratio determined by XPS at 18 atoms/nm^2 decreases considerably when molybdenum is present. At higher Mo + V loadings, 45MoVA, the atomic ratio is 0.26, very similar to that of 18MVA, which confirms that these loadings are above monolayer. It is interesting to note that aluminum visibility to XPS is significantly higher than that expected for alumina-supported oxides above monolayer. Bulk MoVAl oxide exhibits a (Mo + V)/Al atomic ratio of 2.65, which is above the stoichiometry of the system.

3.4. Methanol TPSR profiles

Table 4 summarizes the methanol TPSR data on alumina-supported catalysts. This table shows the area and T_{max} values of the profiles of formaldehyde, DME and CO produced. The activity of all the catalysts is essentially redox (HCHO) since negligible amounts of DME form. CO_2 forms at much higher temperature. The temperature at which HCHO formation begins (T_{onset}) is also indicated, since this is the principal reaction product. Vanadia on alumina produces more formaldehyde than molybdena on alumina, which is in line with the higher redox properties of surface vanadia; also the T_{onset} is lower for 18VA. The formaldehyde production is highest when both Mo and V are present (18MoVA); in addition, 18MoVA exhibits the lowest T_{onset}. The formaldehyde production decreases as Mo + V loading increases to 45MoVA, being T_{onset} significantly higher.

4. Discussion

Taking into consideration that the main XRD phase is $AlVMoO_7$ (Fig. 1a), and that the only unknown Raman phase of the bulk-MoVAl sample presents bands at 761, 231 and 203 cm^{-1} (Fig. 2a), it can be deduced that these three bands belong to the mixed $AlVMoO_7$ phase. The intense Raman bands of $Al_2(MoO_4)_3$ phase, not detected by XRD, indicate that (a) the dominions of $Al_2(MoO_4)_3$ are below 4 nm and, thus do not generate a diffraction pattern; (b), that the Raman section of $AlVMoO_7$ is much lower than that of $Al_2(MoO_4)_3$. Further confirmation of this assignment is found on the Raman spectra of bulk MoVAl-48 (Fig. 2b), where the Raman bands of $Al_2(MoO_4)_3$ increase with respect to those of $AlVMoO_7$, in line with XRD results. Therefore, the Raman bands of $AlVMoO_7$ are reported for the first time, to the best of our knowledge.

The Raman analysis is rather qualitative, since the Raman intensity of the different phases depend on their Raman section, which is much weaker for the new phase $AlVMoO_7$ than for $Al_2(MoO_4)_3$, V_2O_5 and MoO_3. However, it complements XRD characterization for it is sensitive to crystalline particles smaller than 4 nm and amorphous phases. Thus, it is possible to observe domains of $Al_2(MoO_4)_3$ in bulk MoVAl-24 (Fig. 2a) that are too small to generate a diffraction pattern (Fig. 1a). Table 2 lists the phases observed by XRD and Raman spectroscopy in the reference and catalysts.

The chemistry of the Mo–V–Al oxide system is rich and rather complex: the works by Kurzawa and Drawoska show that it is a very dynamic system [18,25,26]. In the three-component system Al_2O_3–V_2O_5–MoO_3, each of the components are reactive towards each other in the solid state; the phases can enter into reaction depending on the molar proportion of the mixture and this causes the appearance of various solid phases, such as $AlVMoO_7$ and $V_9Mo_6O_{40}$; $AlVMoO_7$ and $V_{2-2x}Mo_xO_{5-2x}$; $AlVO_4$ and $V_{2-2x}Mo_xO_{5-2x}$. Among these, $AlVMoO_7$ phase dominates in a wide range of temperatures and compositions [25,26]. Under our synthesis conditions (calcination temperature 550 °C for 5 h), $AlVMoO_7$, $Al_2(MoO_4)_3$ and $V_9Mo_6O_{40}$ dominate for V:Mo:Al = 1:1:1, which would apply for the bulk samples. In our case, we observe the presence of $AlVMoO_7$ and $Al_2(MoO_4)_3$, but no evidence of $V_9Mo_6O_{40}$ by XRD or Raman. V and Mo are not at their maximum oxidation state in $V_9Mo_6O_{40}$, and XPS show that V and Mo are essentially as Mo^{6+} and V^{5+}. Therefore, this phase is not present in our system. It should be noted that upon treatment at 600–700 °C, the system exhibits only $AlVMoO_7$ and $Al_2(MoO_4)_3$. These trends are consistent with those observed in the bulk MoVAl phase.

Works by Lambert et al. prove that a strong metal-support interaction takes place in the deposition stage by surface dissolution followed by reaction in the liquid phase when using anionic precursors such as molybdate [27]. These works have shown the formation of an Anderson type heteropolyanion: $(NH_4)_3[Al(OH)_6Mo_6O_{18}]$ when contacting γ-Al_2O_3 with an aqueous solution of heptamolybdate due to a substancial dissolution of the alumina support and the subsequent

complexation between dissolved Al^{3+} and $Mo_7O_{24}{}^{6-}$. This may be related to the formation of $Al_2(MoO_4)_3$.

Aluminum visibility to XPS is lower than the bulk ratio for the reference sample, which would suggest a surface enrichment in Mo and V for the bulk samples. XPS data show that the surface composition near the surface is not like the bulk composition for all the catalysts.

For supported catalysts, XPS shows the formation of aggregates above monolayer for vanadia on alumina, which is structurally confirmed by XRD and Raman spectroscopy. 18VA exhibits a high V/Al atomic ratio determined by XPS (0.44) and its structure is dominated by crystalline V_2O_5 and γ-Al_2O_3. With the same atomic loading, 18MoA exhibits a much lower Mo/Al atomic ratio determined by XPS (0.21). The XPS data underline a remarkable increase of Al visibility in the molybdena–alumina system. The values would not fit in the scope of a system with more than two monolayers on alumina, particularly if we consider that the actual coverage of Mo on alumina at 18 atoms/nm^2 is higher than that for vanadia alumina, since monolayer coverage is lower for molybdena (ca. 5 versus ca. 8 atoms/nm^2) [19].

M/Al XPS ratios are much lower for 18MoA than for 18VA. Structurally, both systems present the oxide support, the supported oxide and a mixed phase. However, literature data show that the interaction between alumina and Mo is very intense [22,23]; much stronger than that with V [16], which requires more energetic conditions to form Al–V–O phases. Molybdenum interacts readily with alumina at high temperatures and also under humid environment at lower temperatures [21]. These interactions lead to a rather easy formation of $Al_2(MoO_4)_3$ in alumina-supported molybdena [22]. Similar trends are observed for group VI element on other supports, like tungsten oxide on alumina [28] or zirconia-supported molybdena [29]. Thus, molybdenum sites strongly promote the solid-state reactivity of Al sites from alumina support at high coverages, which accounts for the decrease of Mo/Al atomic ratio determined by XPS.

The scenario becomes particularly interesting if V and Mo are present along with alumina at high coverage. The M/Al ratios for Mo and V are remarkably low for 18MoVA and 45MoVA (Table 3). These values would not fit under the scope of several layers on alumina. On alumina-supported catalysts, most aluminum sites are inside the support phase. Thus, for the alumina-supported Mo–V oxide catalysts, the exposure of Al sites to Mo and V is much lower than in the bulk V–Mo–Al system, which affects the Al–V–Mo oxide system chemistry. However, Mo triggers the mobility of Al ions, and both catalysts exhibit similar structures, $AlVMoO_7$ and $Al_2(MoO_4)_3$. XPS underlines a migration of Al sites to the Mo/V phases. XRD and Raman spectroscopy provide the structural phenomenon that accounts for XPS data. Mixed phases involving aluminum sites become dominant. In 18MoVA, the system is dominated by $AlVMoO_7$, which accounts for the high Al signal in XPS analyses. As coverage increases to 45MoVA, the Mo–Al interaction appears dominant over the ternary Mo–V–Al interaction (XRD Fig. 1f and Raman Fig. 2f), so that the population of $AlVMoO_7$ decreases in favor of $Al_2(MoO_4)_3$ and some segregated MoO_3 and V_2O_5. The increase of $Al_2(MoO_4)_3$ population (Fig. 1f) is should be consistent with the increase in the V/Al and the decrease of Mo/Al atomic ratios determined by XPS for 45MoVA. Therefore, the bulk structures observed in the alumina-supported Mo–V oxide systems are consistent to those described for the bulk Al–V–Mo oxide system [18,25,26].Methanol TPSR data show that all the catalysts possess essentially redox activity, with HCHO as the main primary product (Table 4). 18VA produces more HCHO than 18MoA, in line with is higher redox properties. In addition, $Al_2(MoO_4)_3$ phase is present in 18MoA; which may account for its much lower reactivity. When half of the V atoms are replaced with Mo (18MoVA), production of HCHO is highest. The higher reactivity, is not only evidently by the higher production of HCHO but also for the significantly lower temperature at which HCHO formation begins, being 125 °C for 18MoVAl, 149 °C for 18VA and 153 °C for 18MoA. Vanadium exposure (XPS) is lower in 18MoVA than in 18VA; therefore, the high activity of 18MoVA must be related to the presence of $AlVMoO_7$ mixed phase, in line with previous works [10,13]. It is not possible to assess the exact nature of the species exposed to the reactants, and it is not possible to exclude the coexistence of surface Mo and V oxide species, their interaction at the surface may account for the higher redox activity, in line with some results on supported V and Mo oxides on alumina for propane ODH, where Mo would promote the adsorption of reactants thus leading to higher conversion values [12]. 18MoVA also exhibits some increase in DME and CO_2 formation, this underlines that some acidic sites become exposed. This is probably due to alumina sites [20], and would be consistent with the high Al exposure determined by XPS. The appropriate equilibrium between V and Mo exposed sites may lead to a more efficient catalytic system, like that observed for 18MoVA (Table 4). This may be closely related to the rich chemistry of the Al–V–Mo oxide system, which may present many phases depending on composition and temperature [18,21], and it may also be sensitive to environmental conditions, which would endow high reactivity to the system.

Reaction condition #2 follow the effect of Mo + V loading on alumina. Comparing the data between reaction conditions #1 and #2 show differences in the total area, due to the different experimental conditions. However, the product distribution is essentially the same. As we increase total Mo + V coverage on alumina, total activity decreases, which is in line to a lower dispersion of the oxide phases, determined by XPS. Thus, the number of exposed sites does not increase with loading, even decreases. 45MoVA presents a decrease in the $AlVMoO_7$ to $Al_2(MoO_4)$ phase population ratio, being the former associated to higher activity and the latter to lower activity. Thus, the methanol TPSR trends are consistent with the structural changes. Thus, an excess of exposed Mo sites would be detrimental for the appropriate equilibrium between V and Mo. In the light of these results it can be concluded that intermediate mixed Mo–V oxide loadings are necessary to control the formation of $AlVMoO_7$ mixed phase as the main phase, which in turn is related to higher activity in oxidation of chemisorbed methanol to formaldehyde.

5. Conclusions

Mixed Mo–V–Al oxide system forms $AlVMoO_7$ and $Al_2(MoO_4)_3$ under our experimental conditions. Molybdenum sites interact strongly with alumina support, facilitating its migration to the supported phase, thus reacting with V and Mo species, leading to $AlVMoO_7$. The Raman bands of $AlVMoO_7$ are reported here for the first time. Alumina-supported Mo–V oxide exhibits similar structural properties than the bulk Al–V–Mo oxide system. Alumina-supported Mo–V oxide system exhibits essentially redox properties, which appear associated to the presence of the $AlVMoO_7$ phase; however, the exact nature of the surface species is not clear.

Acknowledgements

This research was funded by the Spanish Ministry of Education and Science project CTQ2005-02802/PPQ. SJK acknowledges the Comunidad de Madrid for a PhD fellowship. RGL acknowledges CSIC and European Social Fund for a Postdoctoral I3P fellowship.

Reference

[1] E.A. Mamedov, V. Cortés Corberán, Appl. Catal. A: Gen. 127 (1995) 1.
[2] R.K. Grasselli, Catal. Today 49 (1999) 141.
[3] (a) T. Blasco, J.M. López-Nieto, Appl. Catal. A 157 (1997) 117;
(b) P. Botella, J.M. López-Nieto, B. Solsona, A. Mifsud, F. Márquez, J. Catal. 209 (2002) 445;
(c) P. Botella, J.M. López-Nieto, A. Dejoz, M.I. Vázquez, A. Martínez-Arias, Catal. Today 78 (2003) 507.
[4] H.H. Kung, Adv. Catal. 40 (1994) 1.
[5] (a) D. Linke, D. Wolf, M. Baerns, S. Zeyβ, U. Dingerdissen, L. Mleczko, Chem. Eng. Sci. 57 (2002) 39;
(b) D. Linke, D. Wolf, M. Baerns, O. Timpoe, R. Schögl, S. Zeyβ, U. Dingerdissen, J. Catal. 205 (2002) 16.
[6] E.M. Thorsteinson, T.P. Wilson, F.G. Young, P.H. Kasai, J. Catal. 52 (1978) 116.
[7] H. Jiang, W. Lu, H. Wan, J. Mol. Catal. A 208 (2004) 213.
[8] K. Oshihara, T. Hisano, W. Ueda, Top. Catal. 15 (2001) 153.
[9] M.A. Vuurman, D.J. Stufkens, A. Oskam, G. Deo, I.E. Wachs, J. Chem. Soc. Faraday Trans. 92 (17) (1996) 3259–3265, Sep 7.
[10] M.A. Bañares, S.J. Khatib, Catal. Tod. 96 (2004) 251.
[11] M.D. Amiridis, R.V. Duevel, I.E. Wachs, Appl. Catal. B 20 (1999) 111.
[12] B. Mitra, I.E. Wachs, Goutam Deo, J. Catal., in press.
[13] H. Dai, A.T. Bell, E. Iglesia, J. Catal. 221 (2004) 491.
[14] M.O. Guerrero-Pérez, M.A. Bañares, Chem. Commun. (2002) 1292.
[15] L.J. Burcham, L.E. Briand, I.E. Wachs, Langmuir 17 (2001) 6164.
[16] M.V. Martínez-Huerta, G. Deo, I.E. Wachs, J.L.G. Fierro, M.A. Bañares, in preparation.
[17] L.J. Burcham, L.E. Briand, I.E. Wachs, Langmuir 17 (2001) 6164.
[18] M. Kurzawa, G. Dabrowska, J. Therm. Anal. Calorim. 56 (1999) 217.
[19] I.E. Wachs, B.M. Weckhuysen, Appl. Catal. A 157 (1997) 67.
[20] G.G. Cortéz, J.L.G. Fierro, M.A. Bañares, Catal. Today 78 (2003) 219.
[21] M. Kurzawa, G. Dabrowska, Solid State Ionics 101–103 (1997) 1189.
[22] L. Le Bihan, P. Blanchard, M. Fournier, J. Grimblot, E. Payen, J. Chem. Soc., Faraday Trans. 94 (1998) 937.
[23] C. Rocchiccioil-Delfcheff, M. Amirouche, M. Che, J.M. Tatibouët, M. Fournier, J. Catal. 125 (1990) 2892.
[24] D.D. Wagner, W.M. Riggs, L.E. Davis, J.F. Moulder, G.E. Lilenberg, Handbook of X-ray Photoelectron Spectroscopy, Perking-Elmer, Corporation, Eden Prairie, Minnesota, 1978.
[25] M. Kurzawa, G. Dabrowska, J. Thermal Anal. Calorim. 60 (2000) 183.
[26] M. Kurzawa, G. Dabrowska, Solid State Ionics 101–103 (1997) 1189.
[27] X. Carrier, J.F. Lambert, M. Che, J. Am. Chem. Soc. 119 (1997) 10137.
[28] S.S. Chan, I.E. Wachs, L.L. Murrell, N.C. Dispenziere, J. Catal. 92 (1985) 1.
[29] S. Damyanova, M.A. Bañares, J.L.G. Fierro, Chem. Mater. 12 (2000) 501.